Analytical Methods

Cite this: *Anal. Methods*, 2011, **3**, 614

www.rsc.org/methods

PAPER

Ring magnets for magnetic beads trapping in a capillary†

Anne-Laure Gassner,[a] Jacques Morandini,[b] Jacques Josserand[a] and Hubert H. Girault*[a]

Received 5th October 2010, Accepted 6th December 2010
DOI: 10.1039/c0ay00596g

This paper introduces the concept of ring magnets for magnetic beads (MBs) trapping in a capillary. Such magnets enable an easy insertion of a capillary simply like a pearl on a string. With this system, high magnetic forces are obtained thanks to the proximity between the magnet and the capillary, giving the opportunity to work at higher flow rates than with classical setups using two magnets with their magnetization perpendicular to the capillary. Moreover, by alternating magnets and non-magnetic spacers either in attraction or repulsion configuration, it is possible to form a chain and as a consequence to adapt the number of magnets to the desired number of plugs, thus controlling the surface available for molecule binding. Magnetic force mapping was first carried out by numerical simulations for a single ring magnet. The usefulness of this concept was then demonstrated with the achievement of an immunoassay and an online preconcentration experiment. To study the formation of multiplugs, the magnetic force was first simulated for a chain of four magnets in repulsion. This force was then introduced into a convection-diffusion model to understand the influence of the flow velocity on their size and position. The numerical simulations were qualitatively corroborated by microscopic visualizations, carried out in a capillary placed between rectangular magnets having a magnetization parallel to the capillary, and quantitatively by bead capture efficiency experiments.

1 Introduction

Magnetic beads (MBs) have now proven to be a powerful tool in both research and biomedical applications. They are available in a wide range of sizes (from nm to several μm) and their surface can be modified with molecules having biological specificities and functions.[1–3] The large choice of functionalisation developed over the last few years covers non-specific interactions, such as ionic or hydrophobic ones, as well as group-specific interactions, like immobilized metal affinity chromatography (IMAC) and, finally, specific interactions such as antigen–antibody.[4] In microfluidics, where the goals are faster reaction time and reduced sample consumption, MBs offer many advantages. Firstly, compared to an open microchannel, a packed bed of beads increases the specific surface available for molecule binding. The diffusion pathway is significantly reduced, improving interactions between molecules. Moreover, in comparison to classical beads, they can be easily manipulated by electromagnets or permanent magnets.[5] For these reasons, they have been used for many biological purposes in microfluidics, such as cell manipulation,[6–9] protein immunocapture,[10–12] online preconcentration,[13] in-line extraction,[14] support for on-chip enzymatic digestion,[15,16] DNA hybridization,[17,18] DNA microfluidic electrophoresis through magnetic bead columns[19] or immunoassays.[20–26]

Depending on the magnetic field pattern, strength and gradient required, there are different ways to use magnets in conjunction with a microsystem. The classical and most widely used method involves placing macro-sized external magnets, either permanent (for example made of neodymium iron boron (NdFeB)) or electromagnets close to a microchip. Both provide relatively large magnetic fields (0.5–1 T), but they are rather bulky and lack confined spatial control. Electromagnets present additional attractive features compared to permanent magnets, as they can be switched on and off, and their magnetic field can be tuned. However, for a given size, they produce smaller magnetic fields than permanent magnets. Another option consists of integrating microfabricated electromagnets into the microchip with the advantage of local addressability. This enables the magnets to be positioned very close to the microchannel, thus reducing the need for the field strength, but also requires complex microfabrication techniques, which can be time consuming. Moreover the field strength remains limited (mT

[a]*Ecole Polytechnique Fédérale de Lausanne, Laboratoire d'Electrochimie Physique et Analytique, EPFL SB ISIC LEPA, Station 6, CH-1015 Lausanne, Switzerland. E-mail: hubert.girault@epfl.ch; Fax: +41 21 6933667; Tel: +41 21 6933145*
[b]*Laboratoire LJK, groupe EDP, Université Joseph Fourier, 51 rue des Mathématiques, 38041 Grenoble, France*

† Electronic supplementary information (ESI) available: ESI 1: Finite-element formulation of the magnetic field ESI 2: Finite-element formulation of the species concentration ESI 3: Immunoassay protocol ESI 4: Description of the Plexiglas holder for MBs plugs imaging ESI 5: Parametric study with one magnet ESI 6: Four magnets system (thickness of the spacers) ESI 7: Saturation magnetization in attraction configuration ESI 8: Concentration isovalues versus the apparent diffusion coefficient ESI 9: Comparison of 2D and axisymmetrical simulations. See DOI: 10.1039/c0ay00596g

range).[2,5,18] In order to compensate for the shortcomings of the previous options, magnetic elements magnetized by an external magnet have been integrated into the microchip. The magnetic field is larger than that produced with integrated microelectromagnets and the resulting local magnetic field gradient is increased. Studies have reported the use of permanent magnets in combination with a soft magnetic NiFe material,[27] with permalloy elements,[18] with a magnetic ink containing carbon ink and iron particles[28] and, finally, a ferromagnetic Ni micropost in the middle of the loop of a microelectromagnet,[29] Two theoretical analyses have also described the combination of soft magnetic elements and permanent magnets. The first is an analytical model for the capture and transport of magnetic particles in a magnetophoretic system.[30] The second presents numerical simulations of an external array of mm-sized permanent magnets magnetizing on-chip permalloy magnetic structures.[31]

Multiplugs of MBs have not often been discussed in the literature. Smistrup *et al.* created a microarray with fluorescent and non-fluorescent MBs on each side of a microchannel by using on-chip current lines and hydrodynamic focusing.[32] In another study, the same group used an array of soft magnetic elements magnetized by an external magnet, combined with hydrodynamic focusing to immobilize different types of functionalized beads at the sidewalls of a microchannel to realize hybridization experiments.[18] More recently, magnetic ink tracks coupled to a permanent magnet were developed in our lab, leading to MBs multiplugs filling the entire volume between the ink tracks.[28] All these studies make use of microfabrication techniques requiring time and clean room facilities. Consequently an array of permanent magnets would be a low-cost solution accessible to everyone. To the best of our knowledge, however this possibility has not often been considered. For example, the work of Bronzeau and Pamme used three pairs of permanent magnets, in attraction configuration, to form three plugs of MBs with different functions to carry out simultaneous bioassays.[33]

One can note that numerical simulations regarding the magnetic force and flow in microsystems are not numerous. MBs were treated as a continuum to predict particle concentration distributions[34] or to study their capture in a microchannel.[35] Other studies concern the motion[36] or 3D trajectories of MBs.[29,37]

The present investigation introduces the concept of ring magnet for trapping MBs in a capillary. A disk permanent magnet having axial magnetization is drilled along its magnetization axis. The hole enables the insertion of a capillary simply like a pearl on a string. The axial symmetry and the proximity between the magnet and the capillary produce high magnetic forces, giving the opportunity to work at higher flow velocities than with setups classically made up by two magnets 1 mm apart with their magnetization perpendicular to the capillary. Moreover it is possible to form a chain of disk magnets alternating with disk non-magnetic spacers, placed either in attraction or in repulsion. Finally, it is possible to adapt the number of magnets to the desired number of plugs, increasing in a controllable manner the surface available for molecule binding. This system has the advantage of being very simple to assemble, while keeping a high magnetic force enabling reduced experimental times.

Using numerical simulations, we mapped the magnetic force for a ring magnet. An immunoassay and an online preconcentration were then performed to exemplify the use of such a magnet. To introduce the concept of multiplug, we simulated the magnetic force for a chain of four magnets in repulsion. This force was then introduced into a convection–diffusion model to understand the formation of the multiplugs and the influence of the flow velocity on their size and position. As a qualitative demonstration, the accumulation of MBs was visualized by microscopy in a capillary placed between rectangular magnets having a magnetization parallel to the capillary. Finally, bead capture efficiency was studied as a quantitative proof of concept.

2 Materials and methods

2.1 Numerical models

Numerical simulations, based on the finite elements method (FEM), were carried out with the commercial software Flux-Expert™ (Astek Rhône-Alpes, Grenoble, France) on a Mac Pro with Ubuntu Linux 7.10 operating system. An axisymmetrical problem was studied by two models. The first one involved the simulation of the magnetic field and force distribution, with and without saturation of the MBs. The second coupled magnetism with microfluidics by injecting the magnetic force into the convection–diffusion equation, assuming that the MBs concentration has no influence on the magnetic field distribution.

2.1.1 Magnetic force. The magnetic model has already been discussed in previous studies.[28,38] In the case of permanent magnets and in the absence of charges in movement, the magnetic field $\boldsymbol{H}$ is irrotational and as the calculation domain is simply connected, $\boldsymbol{H}$ derives from a scalar magnetic potential ϕ ($\boldsymbol{H} = -\nabla\phi$). As the magnetic flux density $\boldsymbol{B}$ is conservative, the equation to be solved (using a Galerkin formulation, ESI 1†) is written as:

$$\mathrm{div}\ \boldsymbol{B} = \nabla \cdot (-\mu\nabla\phi + \boldsymbol{B_0}) = 0 \quad (1)$$

where $\boldsymbol{B_0}$ represents the magnetic flux density imposed in the magnet and μ the permeability. The magnetic force $\boldsymbol{F_{mag}}$ acting on a superparamagnetic particle is dependent on $\boldsymbol{B}$ and the bead magnetic dipole moment $\boldsymbol{m}$ by the following relation. The second part of the equation holds if we consider $\boldsymbol{m}$ as a point like magnetic dipole.

$$\boldsymbol{F_{mag}} = \nabla(\boldsymbol{m} \cdot \boldsymbol{B}) \cong (\boldsymbol{m} \cdot \nabla)\boldsymbol{B} \quad (2)$$

We assume that the particle is uniformly magnetized and that the magnetization is a linear function of the magnetic field under an $\boldsymbol{m_{sat}}$ saturation value, for which $\boldsymbol{m}$ becomes constant and equal to $\boldsymbol{m_{sat}}$. Thus the magnetic dipole moment can be written as:[27,39]

$$\boldsymbol{m} = \frac{V\chi}{\mu_0}\boldsymbol{B} \quad (3)$$

with V being the volume of the superparamagnetic particle, χ its effective magnetic susceptibility and μ_0 the permeability of free space. Considering the linear and constant parts of the MBs magnetization curve, two approximations can be made:[39]

(a) if $\boldsymbol{B} < \boldsymbol{B}_{sat}$ ($\boldsymbol{B}_{sat}$ being the value of $\boldsymbol{B}$ corresponding to $\boldsymbol{m}_{sat}$), the magnetic moment is proportional to $\boldsymbol{B}$, because located in the linear region of the magnetization curve. Eqn (2) becomes:

$$\boldsymbol{F}_{mag} = \frac{V\chi}{\mu_0}(\boldsymbol{B} \cdot \nabla)\boldsymbol{B} \quad (4)$$

(b) if $\boldsymbol{B} \geq \boldsymbol{B}_{sat}$, such as $\boldsymbol{m} = \boldsymbol{m}_{sat}$, we have:

$$\boldsymbol{F}_{mag} = (\boldsymbol{m}_{sat} \cdot \nabla)\boldsymbol{B} \quad (5)$$

The following assumptions are made: (a) magnetostatic conditions ($\partial\boldsymbol{B}/\partial t = 0$ and no external source of electric or magnetic field), (b) homogeneous media (μ uniform everywhere), (c) air box big enough not to perturb the magnetic field distribution, (d) constant magnetic susceptibility of the MBs, (e) static bead solution in the microchannel (no flow), (f) MBs have no influence on the magnetic field and (g) interactions between MBs are not considered.

2.1.2 Beads transport and magnetic force coupling. In a capillary, MBs are submitted to a hydrodynamic drag force $\boldsymbol{F}_{drag}$, defined by Stokes' law. The gravitational and particle-fluid forces are neglected. At equilibrium, the drag force is equal to the magnetic force $\boldsymbol{F}_{mag}$, defining a magnetically induced velocity $\boldsymbol{v}_{mag}$.[34,40]

$$\boldsymbol{v}_{mag} = \frac{\boldsymbol{F}_{mag}}{6\pi\eta r} = \frac{V\chi}{6\pi\eta r\mu_0}(\boldsymbol{B} \cdot \nabla)\boldsymbol{B} \quad (6)$$

where η is the fluid viscosity and r the MB radius. The beads flux density N in eqn (7) expresses the respective diffusion, convection and magnetic migration terms (migration by analogy with the electrical migration). The local form of flux conservation is given by:

$$\text{div}\,(N) = \text{div}\left[-D\nabla c + (\boldsymbol{v}_{flow} + \boldsymbol{v}_{mag})c\right] = -\frac{\partial c}{\partial t} \quad (7)$$

where D is the apparent diffusion coefficient, c the bead solution concentration and $\boldsymbol{v}_{flow}$ is the parabolic flow velocity. The integration on the study domain using the Galerkin formulation is described in ESI 2†.

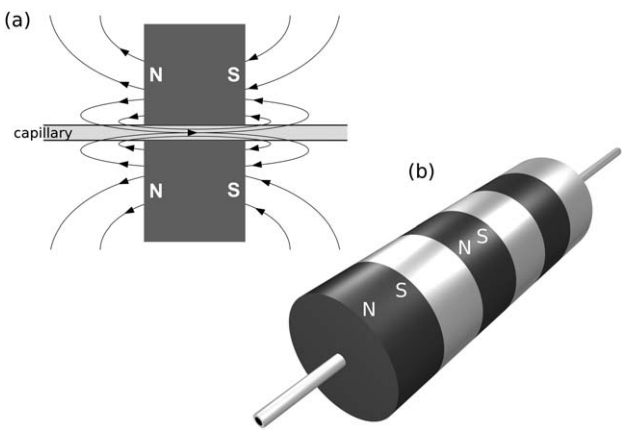

Fig. 1 (a) Scheme of the magnetic field lines in a ring magnet with magnetization parallel to the capillary. (b) Ring magnet "pearl necklace" on a capillary with the magnets in dark grey and the spacers in grey.

2.2 Numerical parameters

The concept of this study is the use of ring magnets for MB trapping in a capillary. Fig. 1a represents the magnetic field lines produced by a ring magnet with a capillary passing along its magnetization axis. A chain of alternating ring magnets and non-magnetic ring spacers with magnets in dark grey and spacers in grey is shown in Fig. 1b. A single magnet was first simulated to study geometrical effects. The interactions between magnets and the fluidic part were then investigated only with four magnets in series. Fig. 2a represents a capillary with an internal radius r_{int} (50 μm) and an external radius r_{ext} (187.5 μm) surrounded by a drilled magnet. It is defined by its thickness t and the parameter Δr_{mag}, which is the difference between its external ($r_{mag.ext}$) and internal ($r_{mag.int}$) radius. The system is placed in an air box, surrounded by an additional air layer using infinite elements that dilate coordinates (*i.e.* the area between the double external lines in Fig. 2a), enabling the magnetic field to rotate freely from one pole to the other. Moreover, parameter d (Fig. 4a) corresponds to the distance between two magnets (thickness of the non-magnetic spacer).

The numerical parameters are: $r_{int} = 50$ [μm], $r_{ext} = 187.5$ [μm], $\mu_0 = 1.256 \times 10^{-6}$ [H m^{-1}], $\boldsymbol{B_0}$ (parallel to the capillary) = ±1 or

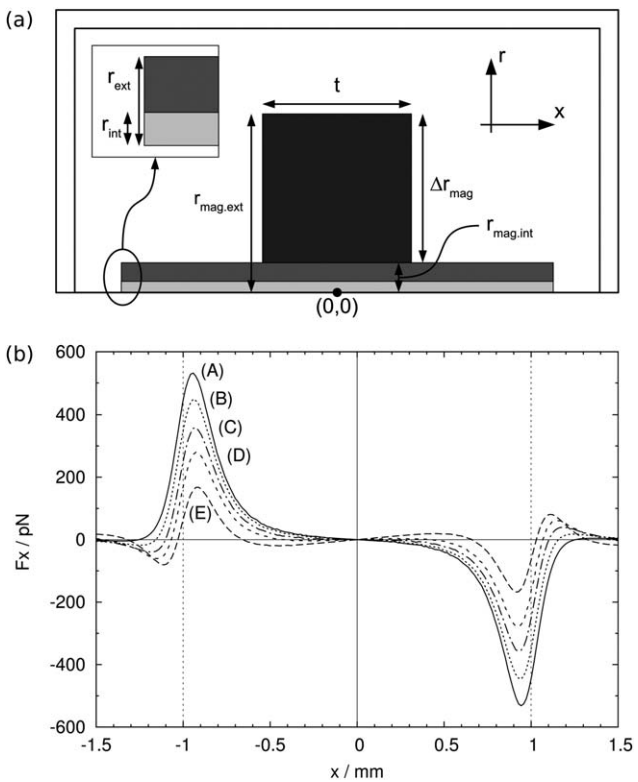

Fig. 2 (a) System composed of a capillary with internal radius r_{int} and external radius r_{ext} surrounded by one permanent ring magnet (dark grey) defined by the difference between its external and internal radius Δr_{mag} and its thickness t. The frame represents the infinite air box. (b) Variation of the magnetic force (x component) for a ring magnet as the function of the ratio $\Delta r_{mag}/t$ ($r_{mag.int} = 187.5$ μm and $t = 2$ mm). $\Delta r_{mag}/t$ ratios: (A) 5, (B) 2.5, (C) 1.5, (D) 1 and (E) 0.5. The forces were calculated for a bead of radius = 500 nm and $\boldsymbol{B_0} = 1$ T. All the values are taken along the x-axis. The vertical dashed lines show the magnet position.

± 1.3 [T], $\chi = 1$ [−], $r = 500$ [nm] or 150 [nm], $\boldsymbol{B}_{sat} = 0.1$ [T] and $c_0 = 1$ [mM].

2.3 Chemicals

Rabbit antibovine β-lactoglobulin polyclonal antibody (1 mg ml^{-1}) was obtained from Gene Tex (Irvine, USA). β-Lactoglobulin from bovine milk was purchased from Sigma (Buchs, Switzerland). Acetic acid (99.5%) and fluorescein sodium were supplied by Fluka (Buchs, Switzerland) and ammonium acetate (98%) by Merck (Darmstadt, Germany). Trifluoroacetic acid (99%) and hydroxypropylcellulose (HPC) were purchased from Acros (Chemie Brunschwig AG, Basel, Switzerland). Acetonitrile was obtained from Riedel-de-Haën (Seelze, Germany). All solutions were prepared with water produced by an alpha Q Millipore System (Zug, Switzerland).

Fused-silica capillaries (75 or 50/375 μm i.d./o.d.) were obtained from BGB Analytik AG (Böckten, Switzerland). Protein-A coated superparamagnetic beads (300 nm diameter) were purchased from Ademtech (Pessac, France) and RPC 18 Dynabeads from Invitrogen. Protein-A bead suspensions were sonicated and diluted 20 times in water. The RPC 18 beads were diluted 10 times, washed three times with TFA 0.1% and then resuspended in TFA 0.1%.

The rectangular permanent magnets used in this study are NdFeB $5 \times 5 \times 1$ mm^3 (Supermagnete, Switzerland). The drilled disk magnets are NdFeB, 10 mm in diameter and 1 mm thick (Supermagnete, Switzerland). They are all magnetized in their smallest dimension, with a magnetic remanence of 1.32–1.36 T for the rectangles and 1.17–1.21 T for the disks.

2.4 Immunoassay and online preconcentration

One ring magnet 1 mm thick was used to carry out the immunoassay. The procedure was adapted from Chen *et al.*[22] The capillary (50/375 μm i.d./o.d., 30 cm effective length, 40 cm total length) was coated with HPC following the procedure described by Shen and Smith[41] to limit as much as possible the EOF and sample adsorption. Protein-A coated MBs were trapped into a HPC coated capillary as a support for antibovine β-lactoglobulin. After binding the antibody on the beads, β-lactoglobulin was immunocaptured and preconcentrated online. Then, acidic conditions were used to dissociate the immunological complex and the respective antibody and antigen were stacked by transient ITP and further separated by CZE. The procedure is described more in detail in ESI 3†. The binding, leading and sample buffers are ammonium acetate (100 mM, pH 8). The elution and separation buffers are acetic acid (10% v/v).

The online preconcentration made use of eight drilled magnets 1 mm thick forming, by magnetic attraction, a large drilled magnet (10 mm in diameter and 8 mm thick). A capillary 75/375 μm i.d./o.d., 40 cm effective length, 50 cm total length was used. A standard fluorescein solution (pH 3) was used as a test molecule. It was adsorbed on the RPC 18 beads and then eluted by flowing an ACN/H_2O solution (50%/50%).

A PACE MDQ system (Beckman-Coulter, Nyon, Switzerland) equipped with a photo-DAD and an autosampler was used for both applications.

2.5 Experimental studies of plug formation

As it is not possible to image plugs within the drilled cylindrical magnet chain, rectangular magnets (magnetization parallel to the capillary) were placed on each side of the capillary to enable a top visualization of MBs accumulation. The permanent magnets were fixed in a Plexiglas holder, described in detail in ESI 4†. In order to demonstrate the approach, quantification of bead capture efficiency was then carried out with the drilled magnets. A PACE MDQ system (Beckman-Coulter, Nyon, Switzerland) equipped with a photo-DAD and an autosampler was used in pressure mode for solution delivery. All the experiments were carried out at a constant (time × pressure) product. To allow the visualization of the beads in transmission, the external polyamide layer of the 1 m long capillary was removed on a 2 cm long window. The observation was carried out with a microscope Axiovert 200 (Carl Zeiss, Göttingen, Germany) and a CCD-IRIS camera (Sony, Tokyo, Japan). The magnets were set in place before flowing the MBs through the capillary.

To quantify the bead capture efficiency, the protocol involved 3 steps: MBs loading and trapping, capillary rinsing to remove all the non-trapped MBs and finally MBs removal by a 50 psi pressure application. The area of the peak detected by DAD was determined. All experiments were repeated at least 3 times in order to evaluate the reproducibility.

3 Results and discussion

3.1 Single ring magnet

3.1.1 Magnetic force simulations. The first part of this work concerns the effect of geometrical parameters on the magnetic force for a single ring magnet. The influence of the internal radius of the magnet $r_{mag.int}$ and the ratio $\Delta r_{mag}/t$ was studied. The results of the internal radius of the magnet are presented in ESI 5† and Fig. 2b evaluates the effect of the ring magnet's shape. Keeping the thickness constant ($t = 2$ mm) and $r_{mag.int} = 187.5$ μm, Δr_{mag} was varied to give $\Delta r_{mag}/t$ ratios between 0.5 and 5. The value of the magnetic force x component was plotted along the x-axis. The magnetization is parallel to the capillary. As for rectangular magnets with a magnetization perpendicular to the microchannel,[38] two magnetic force peaks (positive and negative) are obtained inside the magnet borders, generating a plug in the magnet centre. It can be observed that an increase in this ratio produces an increase in the magnetic force. Relative to the $(\boldsymbol{B} \cdot \nabla)\boldsymbol{B}$ term, this effect is mainly due to an increase in the magnetic flux density value in the magnet hole with the $\Delta r_{mag}/t$ ratio (see ESI 5† for $\boldsymbol{B}$ isovalues).

3.1.2 Immunoassay and online preconcentration. The magnetic force produced by a ring magnet is high due to the proximity between the capillary and the magnet. It is thus possible to work at higher pressure than with two magnets placed on each side of the capillary. As explained in the Materials and methods section, the procedure presented by Chen *et al.* for the performance of their immunoassay is relatively long. Increasing the working pressure could reduce the experimental time, but in their case the beads are removed at 69 mbar already. Working with ring magnets may solve this problem. Fig. 3a presents the

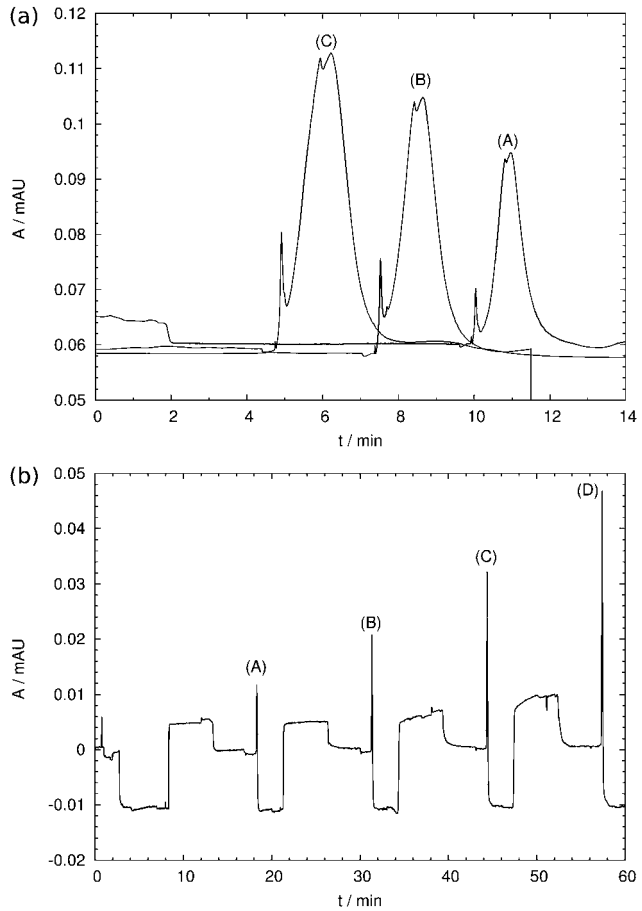

Fig. 3 (a) Evolution of the immunoassay signal in relation to the pressure in a 50 μm i.d. capillary. (A) 1 psi, (B) 2 psi and (C) 5 psi. (b) Evolution of the fluorescein elution peak in relation to the solution concentration in a 75 μm i.d capillary with (A) 5 mg l^{-1}, (B) 10 mg l^{-1}, (C) 25 mg l^{-1} and (D) 50 mg l^{-1}.

results obtained with 1 psi (69 mbar), 2 and 5 psi with a β-lactoglobulin concentration of 0.1 mg ml^{-1}. The experimental procedure is the same for the three curves, *i.e.* the injection time of antibody and antigen is the same, but with different pressures. It can be clearly seen that the antibody peak grows up with the pressure, which is straightforward because the injected volume is bigger. No magnetic beads were removed during these experiments, even at 5 psi, proving that the beads are strongly trapped. Working at high pressures enables shorter rinsing times, reducing noticeably the assay time.

Eight ring magnets stuck together have been used to increase the surface available for fluorescein trapping. RPC 18 beads were injected at 4 psi for 1 min. After a rinsing step, fluorescein was adsorbed on the beads. After a second rinsing step, it was eluted by flowing an ACN/H_2O solution (50%/50%). Consecutive loading–elution experiments were carried out with different fluorescein concentrations (5, 10, 25 and 50 mg ml^{-1}) and are presented in Fig. 3b. As the analyte loading time is constant (5 min), the increase in elution peak's height is only due to the different concentration values. Again it is important to notice that the pressure used, 4 psi, is relatively high and again no loss of magnetic beads has been observed.

3.2 Multiple ring magnets

3.2.1 Magnetic force simulations and saturation. A chain of four magnets was then studied in repulsion configuration, while varying the thickness of the spacers (ESI 6†). In repulsion, the magnetization of the rings alternates (NS–SN–NS–SN). The (A) curve of Fig. 4b presents the *x*-component of the magnetic force with a chain of four magnets. This component has a positive value on the left and a negative one on the right of every magnet (shaded), concentrating the beads towards the middle of each magnet. The attraction configuration is discussed in ESI 7†.

The (A) curve of Fig. 4b does not consider MBs saturation. Various $\boldsymbol{B}_{\mathbf{sat}}$ values are cited in the literature: 20 mT for 130 nm diameter particles,[27] 50 mT (800 nm diameter),[34] 100 mT (2.8 μm Dynabeads)[33] and finally the highest value found was 0.3 T and higher.[6] Fig. 4b shows the magnetic force resulting from several saturation magnetic flux densities in repulsion. Logically the

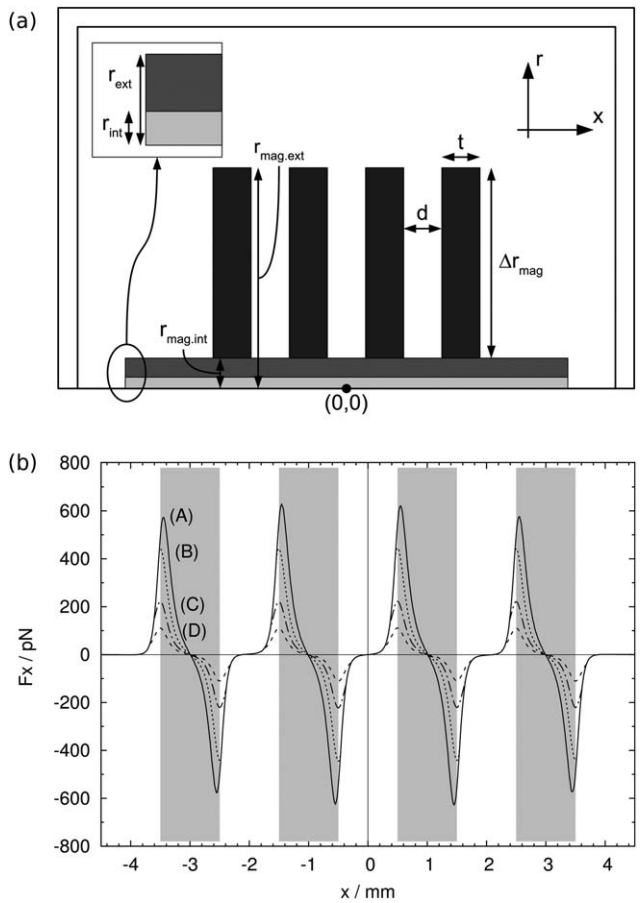

Fig. 4 (a) System composed of a capillary with internal radius r_{int} and external radius r_{ext} surrounded by four permanent magnets (dark grey) defined by the difference between their external and internal radius Δr_{mag} and their thickness *t*. The area between the two external double lines represents the infinite air box. *d* is the thickness of the spacer. (b) Variation of the magnetic force (*x* component) for four magnets in repulsion, for several saturation magnetic flux density $\boldsymbol{B}_{\mathbf{sat}}$. (A) 1 T, (B) 0.4 T, (C) 0.2 T and (D) 0.1 T. The forces were calculated for a bead of radius = 500 nm and $\boldsymbol{B}_{\mathbf{0}} = 1$ T. $r_{mag.int} = 187.5$ μm, $\Delta r_{mag} = 5$ mm, $t = 1$ mm and $d = 1$ mm. All the values are taken along the *x*-axis. The grey surfaces show the position of the four magnets.

magnetic force maxima decrease with $\boldsymbol{B}_{sat}$, but the number of MB plugs and their position remain the same. The magnetic force is divided by a factor of almost 6, when $\boldsymbol{B}_{sat}$ passes from 1 T (corresponding to $\boldsymbol{B}$ imposed in the magnets) to 0.1 T. When considering a $\boldsymbol{B}_{sat}$ of 0.1 T, the magnetic force is slightly above 100 pN. This $\boldsymbol{B}_{sat}$ value will be maintained until the end of this work.

3.2.2 Flow study and microscopic visualizations. To investigate the effect of the parabolic flow on the accumulation of MBs, numerical simulations coupling the species convection–diffusion with the magnetic migration were carried out. The system parameters are the following: Δr_{mag} is 5 mm, t is 1 mm, d is 1 mm, $r_{mag.int}$ is 187.5 μm and four magnets in repulsion are considered. The radius of the beads is 150 nm and $\boldsymbol{B}_0$ is equal to 1.3 T in order to enable qualitative comparisons with the beads and magnets used in the experiments. The apparent diffusion coefficient, representing the repulsion between bead columns, was estimated by comparing the concentration isovalues (ESI 8†) with the experimental visualizations in Fig. 5b. A value of 4×10^{-8} m^2 s^{-1} was chosen.

Fig. 5a shows the final concentration obtained as a function of the flow velocity. At low flow velocities, it can be observed that the concentration peaks are not uniformly distributed. The first peak is larger than the others and the last one is almost nonexistent. It is therefore necessary to increase the flow velocity in order to increase the uniformity of the plugs. But when it is too high, the magnetic force is no longer sufficient to trap all the beads, and many are lost. Therefore the right compromise between the trapping efficiency and the uniformity has to be found. In these simulations, the optimum parabolic flow mean velocity is around 1 mm s^{-1} ($v_{\mathbf{flow\ max}} = 2$ mm s^{-1}). It corresponds to 1.4 times the theoretical magnetic velocity determined from eqn (6) (1.45 mm s^{-1}).

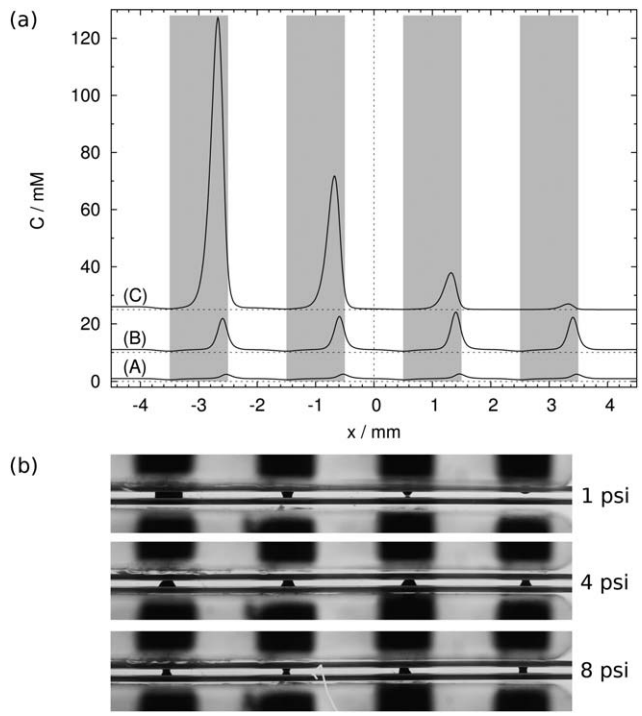

Fig. 5 (a) Concentration profile taken along the x-axis in relation to the flow mean velocity in repulsion configuration. (A) 2 mm s^{-1}, (B) 1 mm s^{-1} and (C) 0.5 mm s^{-1}. The MBs radius is 150 nm and $\boldsymbol{B}_0 = 1.3$ T. The curves were shifted vertically for clarity and the horizontal dashed lines show the zero for each curve. (b) Microscopic visualizations of MBs plugs in a capillary (i.d. 75 μm) in relation to the pressure applied during MBs loading in repulsion. The black surfaces outside the capillary are the rectangular permanent magnets: height = 5 mm (corresponding to Δr_{mag} in an axisymmetric system), $t = 1$ mm and $d = 1$ mm.

To qualitatively illustrate the numerical simulations, microscopic visualizations have been carried out with rectangular permanent magnets placed on both sides of the capillary instead of the drilled magnets, which are impossible to see through. This geometry only approximates the real geometry, but offers a simple and visual way to observe MBs trapping. 2D Cartesian simulations have been performed to complete the axisymmetrical ones and verify the similarity between the two geometries (see ESI 9†). These rectangular magnets were chosen to have the same dimensions as in the flow study. The height of the magnets is equal to Δr_{mag} (5 mm), their thickness t is 1 mm and the spacer thickness d is 1 mm. A CE instrument was used to apply various pressures so as to visualize the plug formation in relation to the flow velocity. Fig. 5b presents plug distributions obtained in repulsion. It can be seen that the number of plugs predicted by the simulations corresponds to what is observed experimentally. Indeed, four plugs are formed, one per magnet.

Pressure has a strong influence on the trapping of the beads, which was already shown by the simulations of Fig. 5a. In the low-pressure case (first image in Fig. 5b), MBs accumulate mainly on the left part of the system (inlet). The magnets located on the right side (outlet) are free from MBs, as they are all trapped before, leading to an irregular plug size. By increasing the pressure, plugs are more uniformly filled (central image in Fig. 5b). But when the pressure is high compared to the magnetic force, this one is not strong enough to trap all the beads and the plugs are smaller.

3.2.3 Magnetic beads capture efficiency. Experiments were first carried out with four drilled magnets placed in repulsion configuration with 1 mm spacers in order to compare the results with the microscopic visualizations. The distribution of the MBs trapped in the capillary cannot be evaluated, but their total amount can be estimated. Beads were loaded at different pressures (2, 4, 6 and 8 psi), keeping the product (pressure × loading time) constant. The capillary was then rinsed to remove all non-trapped beads. Finally, a high pressure (50 psi) was applied to remove the beads and the area of the peak obtained was determined. The experiment was repeated three times for every pressure. Fig. 6a presents the average of the three measurements with the standard deviation. It can be verified that the quantity of beads trapped is high when the pressure is low. When the pressure is increased, the peak area decreases. These results are therefore consistent with the numerical simulation and the microscopic visualizations presented in Fig. 5a–b respectively. The standard deviation is relatively high at 2 psi due to pump technical limitations when the amount of MBs trapped is high.

The second experiment aimed at confirming the hypothesis, which states that the quantity of beads may increase with the number of magnets. In this context, 2, 4 and 8 magnets placed in

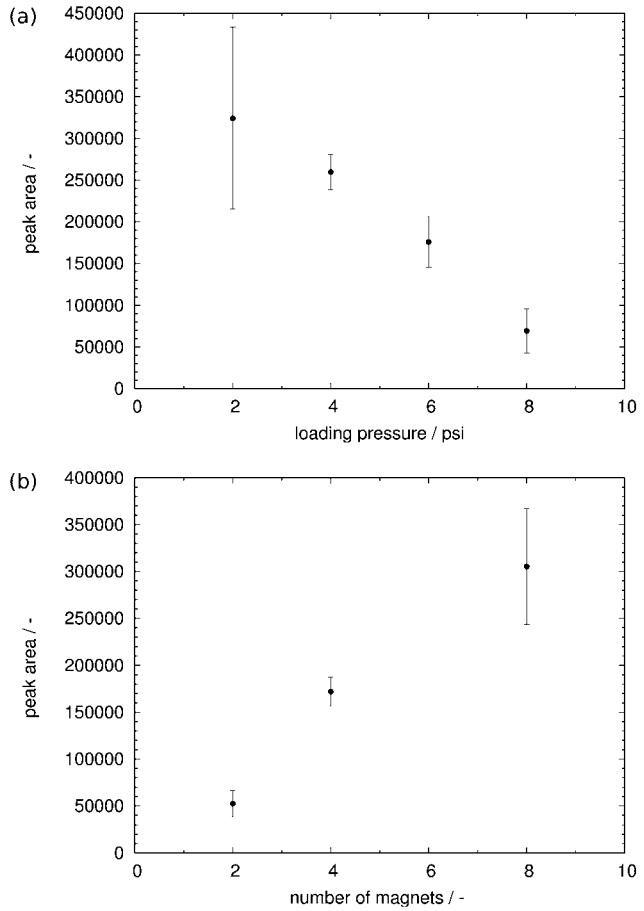

Fig. 6 Evolution of the flushing peak area (415 nm) in a capillary (i.d. 75 μm) for drilled disk magnets in repulsion with 1 mm spacers (a) in relation to the MBs loading pressure ($n = 3$) and (b) in relation to the number of magnets ($n = 4$).

repulsion with 1 mm spacers were used. The same conditions (6 psi, 3 minutes MBs loading) were applied in all the experiments. Four replicates were performed for each number of magnets to calculate the average and standard deviation. The area of the "flushing" peak was determined after the application of a 50 psi pressure. Fig. 6b shows an increase in the peak area, confirming that increasing the number of magnets increases the amount of magnetic beads trapped.

4 Conclusions

Numerical simulations using the finite elements method have been carried out to study ring magnets for trapping MBs within a capillary. A permanent disk magnet having axial magnetization is drilled along its magnetization axis. The hole enables the insertion of a capillary simply like a pearl on a string. First, the magnetic force was mapped for a ring magnet. An immunoassay and an online preconcentration were then performed to exemplify the use of such a magnet. No MBs were lost, even when the pressure was increased up to 5 psi, showing an efficient and strong trapping. The concept of multiplug was then presented by simulating the magnetic force for a chain of four magnets in repulsion. The number of plugs is equal to the number of magnets and MBs are located in the hole of every drilled magnet. Taking into account the MBs saturation leads to a significant decrease in magnetic force, by a factor 6 for a saturation magnetic flux density of 0.1 T (for $\boldsymbol{B}$ imposed in the magnets of 1 T). The multiplugs of MBs are filled successively along the flow direction, but the uniformity of the plugs and the amount of MBs trapped are strongly dependent on the flow velocity. At low flow velocities, many MBs are trapped, but the plugs are not regularly sized, being larger on the inlet than on the outlet side. On the contrary, at high flow velocities, many MBs are lost, the magnetic force being insufficient to trap all the beads, but the uniformity of the plugs is guaranteed. The accumulation of MBs was qualitatively visualized by microscopy in a capillary placed between rectangular magnets, showing the same plug number and position as the numerical simulations. Quantitative bead trapping experiments confirmed that increasing the number of magnets increases the amount of magnetic beads trapped.

Acknowledgements

This work was supported by a Swiss National Science Foundation grant entitled "Supramolecular phases for protein adsorption" (grant no. 404740-117321). Thanks go to Brice Perruche for his technical assistance.

References

1 E. Verpoorte, *Lab Chip*, 2003, **3**, 60N–68N.
2 N. Pamme, *Lab Chip*, 2006, **6**, 24–38.
3 M. A. Gijs, F. Lacharme and U. Lehmann, *Chem. Rev.*, 2010, **110**, 1518–1563.
4 D. Horak, M. Babic, H. Mackova and M. J. Benes, *J. Sep. Sci.*, 2007, **30**, 1751–1772.
5 M. A. Gijs, *Microfluid. Nanofluid.*, 2004, **1**, 22–40.
6 N. Pamme and C. Wilhelm, *Lab Chip*, 2006, **6**, 974–980.
7 I. Safarik and M. Safarikova, *J. Chromatogr., B: Biomed. Sci. Appl.*, 1999, **722**, 33–53.
8 H. Lee, A. M. Purdon and R. M. Westervelt, *Appl. Phys. Lett.*, 2004, **85**, 1063–1065.
9 M. Zborowski, L. P. Sun, L. R. Moore, P. S. Williams and J. J. Chalmers, *J. Magn. Magn. Mater.*, 1999, **194**, 224–230.
10 T. Kaneta, J. Inoue, M. Koizumi and T. Imasaka, *Electrophoresis*, 2006, **27**, 3218–3223.
11 M. Careri, L. Elviri, J. B. Lagos, A. Mangia, F. Speroni and M. Terenghi, *J. Chromatogr., A*, 2008, **O 1206**, 89–94.
12 B. Jankovicova, S. Rosnerova, M. Slovakova, Z. Zverinova, M. Hubalek, L. Hernychova, P. Rehulka, J. L. Viovy and Z. Bilkova, *J. Chromatogr., A*, 2008, **1206**, 64–71.
13 Y. Okamoto, F. Kitagawa and K. Otsuka, *Anal. Chem.*, 2007, **79**, 3041–3047.
14 Y. H. Tennico and V. T. Remcho, *Electrophoresis*, 2010, **31**, 2548–2557.
15 M. Slovakova, N. Minc, Z. Bilkova, C. Smadja, W. Faigle, C. Futterer, M. Taverna and J. L. Viovy, *Lab Chip*, 2005, **5**, 935–942.
16 A. Le Nel, N. Minc, C. Smadja, M. Slovakova, Z. Bilkova, J. M. Peyrin, J. L. Viovy and M. Taverna, *Lab Chip*, 2008, **8**, 294–301.
17 Z. H. Fan, S. Mangru, R. Granzow, P. Heaney, W. Ho, Q. Dong and R. Kumar, *Anal. Chem.*, 1999, **71**, 4851–4859.
18 K. Smistrup, B. G. Kjeldsen, J. L. Reimers, M. Dufva, J. Petersen and M. F. Hansen, *Lab Chip*, 2005, **5**, 1315–1319.
19 N. Minc, C. Futterer, K. D. Dorfman, A. Bancaud, C. Gosse, C. Goubault and J. L. Viovy, *Anal. Chem.*, 2004, **76**, 3770–3776.
20 L. G. Rashkovetsky, Y. V. Lyubarskaya, F. Foret, D. E. Hughes and B. L. Karger, *J. Chromatogr., A*, 1997, **781**, 197–204.
21 M. A. Hayes, N. A. Polson, A. N. Phayre and A. A. Garcia, *Anal. Chem.*, 2001, **73**, 5896–5902.
22 H. X. Chen, J. M. Busnel, A. L. Gassner, G. Peltre, X. X. Zhang and H. H. Girault, *Electrophoresis*, 2008, **29**, 3414–3421.

23 H. X. Chen, J. M. Busnel, G. Peltre, X. X. Zhang and H. H. Girault, *Anal. Chem.*, 2008, **80**, 9583–9588.
24 F. Lacharme, C. Vandevyver and M. A. Gijs, *Anal. Chem.*, 2008, **80**, 2905–2910.
25 R. S. Sista, A. E. Eckhardt, V. Srinivasan, M. G. Pollack, S. Palanki and V. K. Pamula, *Lab Chip*, 2008, **8**, 2188–2196.
26 J. W. Choi, K. W. Oh, J. H. Thomas, W. R. Heineman, H. B. Halsall, J. H. Nevin, A. J. Helmicki, H. T. Henderson and C. H. Ahn, *Lab Chip*, 2002, **2**, 27–30.
27 N. Xia, T. P. Hunt, B. T. Mayers, E. Alsberg, G. M. Whitesides, R. M. Westervelt and D. E. Ingber, *Biomed. Microdevices*, 2006, **8**, 299–308.
28 M. Abonnenc, A. L. Gassner, J. Morandini, J. Josserand and H. H. Girault, *Anal. Bioanal. Chem.*, 2009, **395**, 747–757.
29 B. Le Drogoff, L. Clime and T. Veres, *Microfluid. Nanofluid.*, 2008, **5**, 373–381.
30 E. P. Furlani, *J. Appl. Phys.*, 2006, **99**, 024912-1–024912-11.
31 K. Smistrup, M. Q. Bu, A. Wolff, H. Bruus and M. F. Hansen, *Microfluid. Nanofluid.*, 2008, **4**, 565–573.
32 K. Smistrup, H. Bruus and M. F. Hansen, *J. Magn. Magn. Mater.*, 2007, **311**, 409–415.
33 S. Bronzeau and N. Pamme, *Anal. Chim. Acta*, 2008, **609**, 105–112.
34 K. C. Warnke, *IEEE Trans. Magn.*, 2003, **39**, 1771–1777.
35 C. Mikkelsen and H. Bruus, *Lab Chip*, 2005, **5**, 1293–1297.
36 S. S. Shevkoplyas, A. C. Siegel, R. M. Westervelt, M. G. Prentiss and G. M. Whitesides, *Lab Chip*, 2007, **7**, 1294–1302.
37 P. Pham, P. Massé and J. Berthier, *Eur. Phys. J.: Appl. Phys.*, 2000, **12**, 211–216.
38 A. L. Gassner, M. Abonnenc, H. X. Chen, J. Morandini, J. Josserand, J. S. Rossier, J. M. Busnel and H. H. Girault, *Lab Chip*, 2009, **9**, 2356–2363.
39 Y. Moser, T. Lehnert and M. A. M. Gijs, *Appl. Phys. Lett.*, 2009, **94**, 022505-1–022505-3.
40 N. Pamme and A. Manz, *Anal. Chem.*, 2004, **76**, 7250–7256.
41 Y. Shen and R. D. Smith, *J. Microcolumn Sep.*, 2000, **12**, 135–141.